Design Aspects of an Experimental Setup for Investigating Current Ripple Effects in Lithium-ion Battery Cells

R. Soares[1], A. Bessman[2], O. Wallmark[1], M. Leksell[1], M. Behm[2], and P. Svens[3]

[1] Department of Electrical Energy Conversion, KTH Royal Institute of Technology, Teknikringen 33, SE-100 44 Stockholm, Sweden, E-mail: rudi.soares@ee.kth.see,
[2] Department of Applied Electrochemistry, KTH Royal Institute of Technology,
[3] Scania AB, SE-151 87 Södertälje, Sweden, E-mail: pontus.svens@scania.com,

Acknowledgments

This work was supported in part by the Swedish National Energy Agency.

Keywords

<<Aging>>, <<li-ion battery>>, << ripple>>

Abstract

This paper describes an experimental setup for investigating the effects of current ripple on lithium-ion battery cells. The experimental setup is designed so that twelve li-ion cells can be simultaneously tested in a controlled environment. The experimental setup allows for a wide range of current ripple in terms of frequency and amplitude. Additionally, the quantification of the current ripple effects such as the aging of li-ion cells implies that a precise measurement system has to be designed which also are discussed in the paper.

Introduction

Electric vehicles (EVs), computers, phones, uninterruptible power supplies, among other crucial devices for our society, require the use of an energy source system such as a lithium-ion (li-ion) battery, often combined with a switch-mode power converter (SMPC). Understanding the interaction between li-ion batteries and SMPCs since it can potentially lead to improvements in terms of energy saving, reliability, life expectation and reduced component sizing. Advances in this area would be particularly beneficial in the EV sector where the energy storage system represents the weak element in an electrification of our society's transportation [1].
The effect of ripple currents on li-ion batteries is a relatively unexplored area. It is commonly established that ripple currents reduce the system reliability and the battery life time. As mentioned in [2], ripple currents are often recommended to be limited within specified levels. For this purpose, several techniques, including active or passive filtering design, have been developed to mitigate ripple currents, as exemplified in [3]. However, recent results presented in [4] indicate that ageing is not linked to the applied current ripple. Triggered by this new data, one can naturally question the boundaries of such a statement and, in particular, question the effects of frequency and amplitude of the ripple current when put in different SMPC contexts. Additionally, it has been demonstrated in [5, 6] that by charging a li-ion battery with a specified imposed current ripple, charging efficiency and lifetime expectancy can be improved.
From [2–6], one can conclude that there are different perspectives, as well as different contexts that should be linked together, and questions that should be addressed with appropriate data. With this motivation, an experimental setup, allowing for testing the effect of ripple currents on li-ion battery cells, has been designed and is currently under construction in a joint project of KTH and Scania AB.
In this paper, this experimental setup is described and specific associated challenges and means for mitigation are presented. The outline of the paper is as follows. In Section 1, the li-ion cell in consideration is introduced and the major time-dependent cell effects are described. In Section 2, the experimental

setup is presented. The circuitry used to generate a controlled dc current and superimposed ripple current is discussed and a method to deal with the interaction between multiple frequency passive filters is described. Finally, in Section 3, the measurement techniques and the instrumentation of the experimental setup is discussed. Additionally, reference results for analysing the effects of current ripple in four fresh li-ion cells are characterised and included.

1 Li-ion Cell Effects Depending on Time

In an electrochemical system, such as a battery cell, many different physical and chemical processes interact. Different effects dominate at different timescales, so by exciting the cell by means of ripple currents, and measuring its response at different frequencies, it is possible to differentiate them from each other. Figure 1, based on a previous work by [7], provides a rough outline for which processes dominate at different timescales in a li-ion cell.

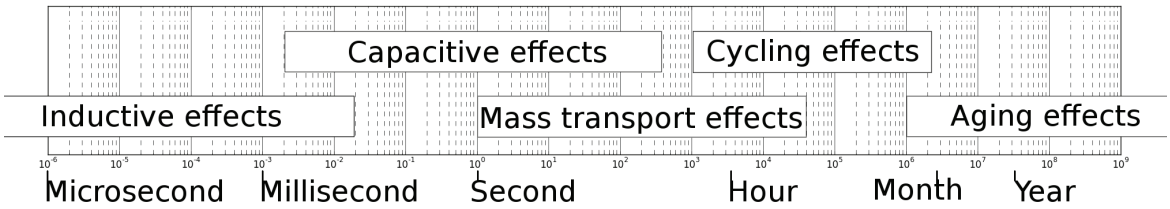

Figure 1: Li-ion cell effects depending on time.

The li-ion cell's characteristics will change with time, usually to the detriment of performance. In simple terms, this means that the li-ion cells will tend to increase their equivalent resistance and lose their equivalent capacity with time. This process is a slow process (months and years) and is termed as aging effects in Figure 1.
Although the term "aging" is reserved to slow processes, one should question the contribution of mass transport, cycling effects, capacitive processes and inductive effects, in the aging process itself. These effects are shown as being distinct and have clearly different timescale footprints. Addressing the ripple current effects in li-ion cells, in separate timescales, is of great interest. For this reason, the experimental setup must cover a wide range of ripple frequencies, and the method selected to run cell characterization measurements is electrochemical impedance spectroscopy (EIS).

2 Experimental Setup

2.1 Experimental Setup Requirements

Prismatic li-ion cells with a charging rate (C-rate) of 25 Ah and a nominal voltage of 3.67 V are considered. The cathode material is Lithium Nickel Manganese Cobalt oxide (NMC) and the anode is graphite. The cells under study are meant to be used in the traction battery of an EV. As shown in [8], in order to minimize the effects of random variations between the cells, large datasets are required. In this sense, for each study case, three cells are studied simultaneously, in order to acquire data with statistical significance.
As mentioned in [9], the temperature has great impact on the aging of li-ion cells. On that account, the temperature has to remain constant, so losses and aging effects are as purely as possible due to the the experimental setup currents. Moreover, since many study cases require long term tests, the experimental setup must be prepared to reach high availability rates, i.e., work uninterruptedly for long periods (i.e., months).
As mentioned in Section 1, a variety of interesting effects are study targets implying that the experimental setup has to be prepared to operate in a wide range of time constants, i.e. frequencies. Moreover, and thinking about the future, it would be of great interest to be able to apply realistic drive cycles to the li-ion cells. Therefore, this aspect is also part of the selected specifications summarized in Table I.
A decisive requirement for the design of the experimental setup was the shape of the current ripple. As demonstrated in [10], for frequencies above 1 kHz, inductive effects in the current collectors and leads become dominant. This means that the exact shape of the ripple is therefore expected to have minimal effect on the aging of the cells. With respect to frequencies lower than 1 kHz, no information is available in the literature. For these reasons, as well as for simplicity, a triangular shaped current ripple was chosen for the first cell tests. Table I summarizes the main experimental setup requirements.

2.2 Direct Current Generator

The experimental setup has been designed such that state of charge (SOC) cycling and ripple current can be produced independently. To attain different SOC cycles, the direct current generator (DCG) was

Table I: Experimental setup requirements

Simultaneous cells	12
Controlled temperature	Yes
Availability	24h - 7days - during months
Programmable SOC	Yes - Drive cycles, etc
dc current	up to 160 A approximately 7 C-rate
Ripple waveform shape	Flexible (triangular, square, etc)
Ripple frequency range	up to 100 kHz
Ripple amplitude range	up to 60 A

adapted from the following battery management unit [11]. The DCG has four independent channels capable of a 40 A dc current each. Also, by combining several channels, the DCG offers the possibility to achieve current levels up to 160 A. In addition, the DCG is prepared to be logged with real data of load cycles. This allows for a great flexibility in studying different SOC cycle profiles as well as different C-rates.

2.3 Current Ripple Generator

A current ripple generator (CRG) has been designed to be used together with the DCG. Figure 2 illustrates the experimental setup. Due to the fact that li-ion batteries in real applications may be used in conjunction with very different SMPC technologies, the CRG has to be flexible and cover a wide range of frequencies and amplitudes. Thus, the CRG is capable of operating at both high ($\sim$100 kHz) and low (a few Hz) frequencies. Also, to cover a wide span of current ripple amplitudes, the CRG is able to produce currents up to 60 A peak-to-peak (almost half of the maximum current delivered by the DCG). To allow the CRG to be superimposed with the DCG, appropriate LCR series filters are used. The CRG is designed for an input voltage of 200 V and using Infineon's IPP220N25NFD MOSFETs. As pointed in Section 1, the equivalent resistance of each li-ion cell will age (i.e., will increase). To compensate this current drift, the CRG's input voltage is controlled using a TDK Lambda controllable power supply Z^{+}-160-4.

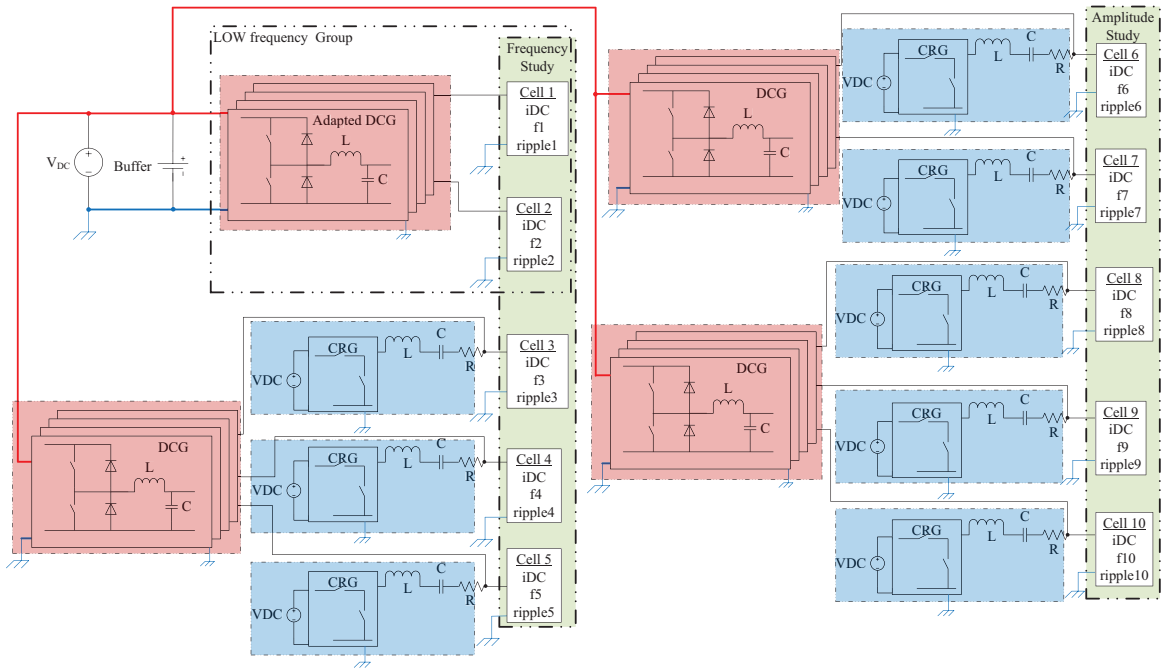

Figure 2: Layout of the experimental setup.

2.4 Filter Design Procedure and Interactions Between Superimposed SMPCs

To carry out a preliminary verification of the experimental setup design, the system has been modeled using MatLab/Simulink[1] and PLECS[2]. The interactions between the LCR filters were revealed to be particulary interesting and therefore will be analysed here.
The experimental setup can be seen as a system where a set of 12 DCGs and 12 CRGs are superimposed. All DCGs and CRGs share the same ground. This means that if not properly designed, the different SMPCs may attenuate each other.
The filter-design process starts by considering each cell's case study and defining its current specifications, i.e. a triangular current with a specified frequency, amplitude and duty cycle. These specifications subsequently define the size of the inductors L_{CRG}. A resistance of $R_{\mathrm{CRG}} = 100$ mΩ is then assumed. To minimize the voltage swing of C_{CRG} during startup, the condition for critical damping

$$\zeta = \frac{R_{\mathrm{CRG}}}{2}\sqrt{\frac{L_{\mathrm{CRG}}}{C_{\mathrm{CRG}}}} = 1 \tag{1}$$

is used from which initial values for C_{CRG} is obtained.
With respect to the DCG filter values, i.e., L_{DCG} and C_{DCG}, the default values are initially kept. However, these values are not suited to optimal superimposition, especially since several CRGs are operated with different ripple current frequency and amplitude specifications. Therefore, the interactions between the CRG and DCG have to be considered in order to select values for L_{CRG}, C_{CRG}, R_{CRG}, L_{DCG} and C_{DCG} so that a triangular shaped ripple current can be accomplished for each battery cell. To analyze these interactions, the battery cells are, initially, considered as comprising only of the an open-circuit voltage in series with a resistance. With this assumption, transfer functions relating different inputs and outputs of system can be derived. For example, the transfer function $G(s)$ from V_{CRGsw} to i_{Cell} (see Figure 3) can be expressed as

$$G(s) = \frac{d_{\mathrm{n}}s^3 + c_{\mathrm{n}}s^2 + b_{\mathrm{n}}s + a_{\mathrm{n}}}{f_{\mathrm{d}}s^5 + e_{\mathrm{d}}s^4 + d_{\mathrm{d}}s^3 + c_{\mathrm{d}}s^2 + b_{\mathrm{d}}s + a_{\mathrm{d}}} \tag{2}$$

where $d_{\mathrm{n}} = C_{\mathrm{CRG}}L_{\mathrm{DCG}}$, $c_{\mathrm{n}} = 0$, $b_{\mathrm{n}} = 0$, $a_{\mathrm{n}} = 0$, $f_{\mathrm{d}} = C_{\mathrm{DCG}}C_{\mathrm{CRG}}L_{\mathrm{DCG}}L_{\mathrm{CRG}}R_{\mathrm{Cell}}$, $e_{\mathrm{d}} = C_{\mathrm{CRG}}L_{\mathrm{DCG}} \cdot (L_{\mathrm{CRG}} + C_{\mathrm{DCG}}R_{\mathrm{Cell}}R_{\mathrm{CRG}})$, $d_{\mathrm{d}} = C_{\mathrm{DCG}}L_{\mathrm{DCG}}R_{\mathrm{Cell}} + C_{\mathrm{CRG}}(L_{\mathrm{CRG}}(k_{\mathrm{p}} + R_{\mathrm{Cell}}) + L_{\mathrm{DCG}} \cdot (R_{\mathrm{Cell}} + R_{\mathrm{CRG}})$, $c_{\mathrm{d}} = L_{\mathrm{DCG}} + C_{\mathrm{CRG}}k_{\mathrm{i}}L_{\mathrm{CRG}} + C_{\mathrm{CRG}} \cdot (k_{\mathrm{p}} + R_{\mathrm{Cell}})R_{\mathrm{CRG}}$, $b_{\mathrm{d}} = k_{\mathrm{i}}R_{\mathrm{CRG}} \cdot (k_{\mathrm{p}} + R_{\mathrm{Cell}} + C_{\mathrm{CRG}})$, $a_{\mathrm{d}} = k_{\mathrm{i}}$.
To minimize the interaction between different battery cells, the corresponding transfer functions are also derived and, through proper selection of the filter parameters, it is ensured that the interaction between different battery cells is minimal. Figure 3 illustrates the corresponding situation. Due to the resulting model complexity, Mathematica[3] is used to obtain the resulting transfer functions.

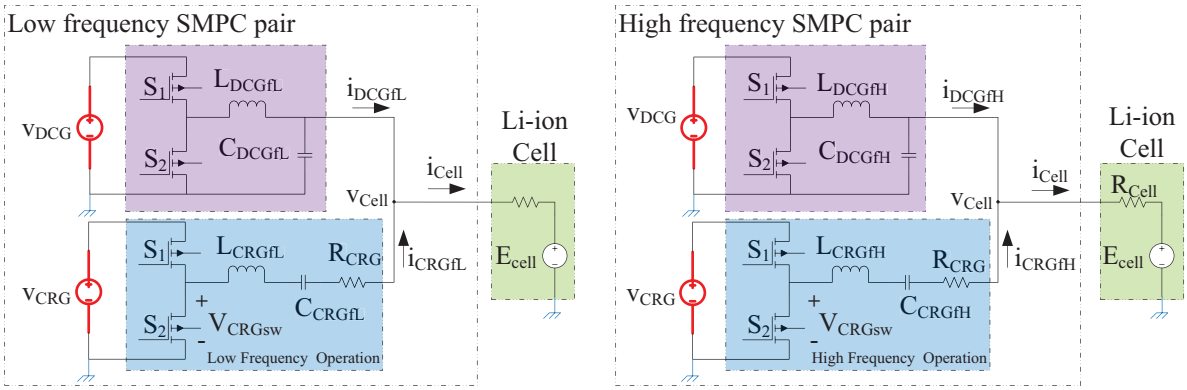

Figure 3: Circuit configuration for a single li-ion cell.

Table II shows the resulting filter values for the DCG and CRG assuming CRG input voltage of 120 V.

[1]Matlab and Simulink are registered trademarks of The Mathworks, Natick, MA, U.S.A.
[2]PLECS is a registered trademark of Plexim GmbH, Zürich, Switzerland.
[3]Mathematica is a registered trademark of Wolfram Research Inc., Champaign, IL, U.S.A.

Table II: Filter values

Cell	Current (A_{pp})	Frequency (kHz)	L_{CRG} (mH)	C_{CRG} (mF)	L_{DCG} (mH)	C_{DCG} (mF)
1	20	0.01	150	41670	31.8	7.9
2	20	0.1	15	4167	3.18	0.79
3	20	1	1.5	417	0.32	0.079
4	20	10	0.15	41.7	0.032	0.039
5	20	100	0.015	4.17	0.0032	0.039
6	5	2	3	833	0.159	0.039
7	15	2	1	278	0.159	0.039
8	30	2	0.5	139	0.159	0.039
9	45	2	0.33	92	0.159	2
10	60	2	2.5	69	0.159	2

2.5 Direct Current Generator Adapted to Work as a Ripple Generator

As seen in Table II, for frequencies below 100 Hz, unreasonable filter-component values would be required. Therefore, for these low frequencies, the DCG has been modified so that besides dc current also a (low-frequency) ripple current could be produced (this is also illstrated in Figure 2). Essentially, an algorithm imposing a "rapid" change of the dc reference current in the DCG is implemented. To test the capability of the DCG to act as a ripple generator, this was replicated in a PLECS simulation environment. The simulation results are shown section 2.6 in Figure 4

2.6 Validation on Ripple Shape Consistency

To verify that a suitable triangular current shape is obtained, the magnitudes of the resulting triangular current is compared to corresponding magnitudes of an ideal triangular waveform. By fixing a specified minimal ripple consistency, the initial values of L_{CRG}, C_{CRG}, R_{CRG}, L_{DCG}, C_{DCG} are then validated or recomputed taking into account the interaction of all SMPCs working simultaneously.

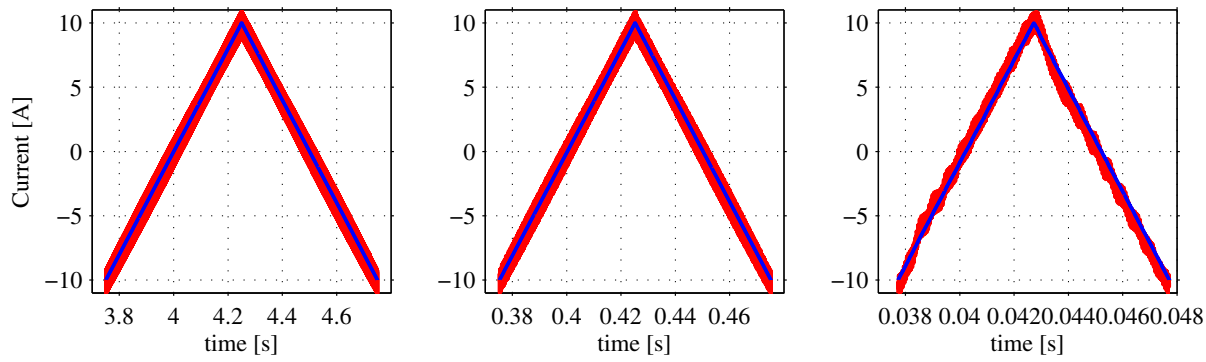

Figure 4: DCG Ripple vs Ideal Ripple for 1, 10 and 100 Hz - in blue the ideal and in red the simulation data

3 Measurements and Instrumentation

3.1 Direct Measurements

Voltage, current and temperature have to be measured in every cell. These three measurements are acquired according to the connections depicted in Figure 6. The core of the acquisition system is a PXI express rack, and its two cards, the PXIe-6124 and the PXIe-8513, from National Instruments. The PXIe-6124 is responsible for acquiring both voltage and current while the temperature is acquired using the PXIe-8513. The PXIe-6124 has an analog input resolution of 16 bits in +/-1V channel, meaning that the voltage measurement has approximately 30 μV of voltage resolution. Additionally, it has a sampling

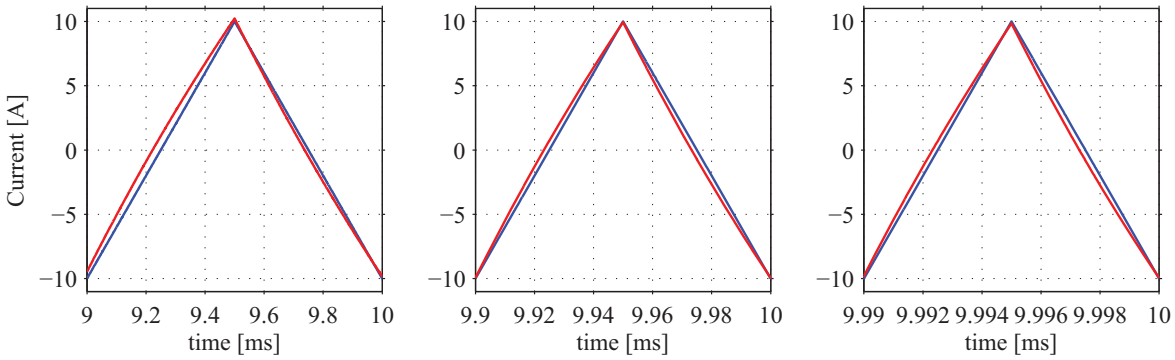

Figure 5: CRG Ripple vs Ideal Ripple for 1, 10 and 100 kHz - in blue the ideal waveform and in red the simulated data

rate of 4 MS/s per channel allowing for sufficient precision when the ripple consistency calculations are preformed.
The cell current is measured in differential mode and transduced as voltage signals using the 3020-01108-0 Murata's dc shunt resistors. As illustrated in Figure 6, voltage and current signals are connected via twisted pairs to a multiplexer which is connected via a very high density cable interconnection (VHDIC) to the PXIe rack. The multiplexer is used for two reasons: the first is that it would be very expensive to have a PXIe-6124 per cell; the second, is that is actually possible to multiplex the signals since the cells are expected to age slowly.
Since the DCG had by default temperature input ports compatible with 10 kΩ negative temperature coefficient (NTC) thermistors, the temperature signals are transmitted via controlled area network (CAN) bus, from the DCG to the The PXIe-8513. Also the PXIe-8513 is responsible for controlling all the DCGs, the CRGs, the multiplexer and the safety system.

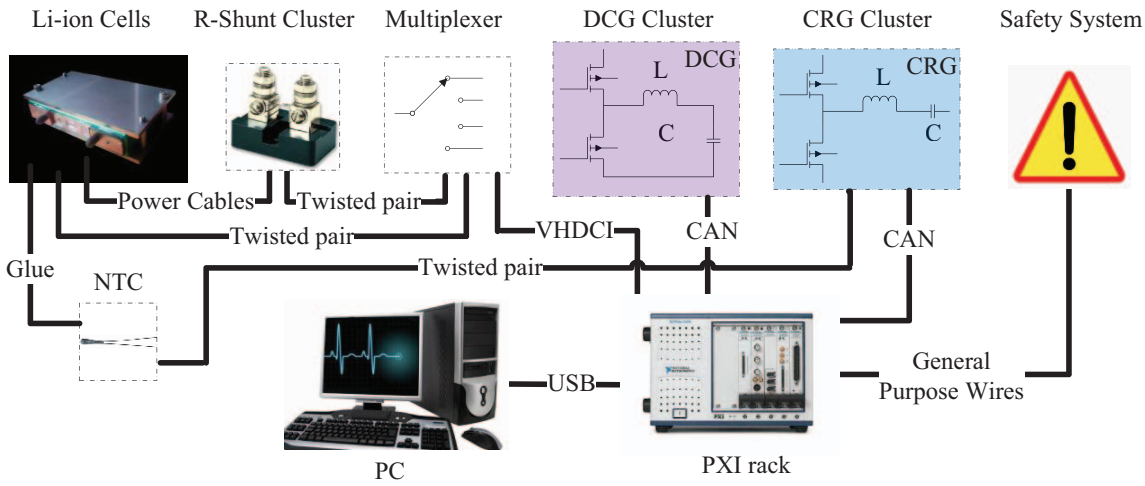

Figure 6: Data acquisition system and associated connections.

3.2 Indirect Measurements

3.2.1 Capacity Characterization and State of Charge control

Since it is desired to follow the progress of the cells' capacity loss over time, it is of importance that the concept of capacity is well defined and that the SOC cycle is precisely controlled. The reason for this need is related with the fact the SOC influences the aging process.

A cell's capacity is the amount of charge which can be used to produce work when the cell is fully discharged from a SOC of 100% all the way down to 0%. For the sake of precision, the capacity must also be defined at a specific current since the higher the current, the more losses will occur both during charge and during discharge. Also, the more losses, the lower the cell voltage will be during discharge (and vice versa during charge). Therefore, the cell capacity is characterized at a current of 25 A, corresponding to 1 C-rate. This is important since the implemented SOC cycle depends on good voltage and current measurements. SOC control is implemented using the following method: the cells are charged with constant current until their voltage exceeds 4.1 V. At this point the voltage is held at that level until the current falls below 1/10 C (2.5 A). At this point the cell is considered as fully charged, i.e. SOC 100%. Then, the cells are discharged with a constant current until their voltage falls below 3.0 V. At this point the cell is considered as fully discharged, i.e. SOC 0%. Since we are only interested in the evolution of total capacity, no SOC levels other than the upper and lower limits are of interest. Therefore, SOC levels other than 0% and 100% are left undefined.

3.2.2 Electrochemical Impedance Spectroscopy (EIS)

As mentioned in Section 1, EIS can be used to distinguish processes which occur on different timescales. EIS data are typically plotted in Bode plots, where the impedance magnitude response is plotted against the frequency, and Nyquist plots, where the real and imaginary parts of the impedance are plotted against each other. Figure 7 shows the EIS data collected from four fresh li-ion cells. Figure 7 a) and Figure 7 b) correspond to magnitude and phase of a Bode plot respectively, while Figure 7 c) corresponds to the same data plotted instead in a Nyquist plot. All impedance data are measured potentiostatically with a current perturbation of 2 A applied. In Figure 7 c), a frequency and effect label is included providing a better perception of the relative importance of different phenomena at different frequencies.

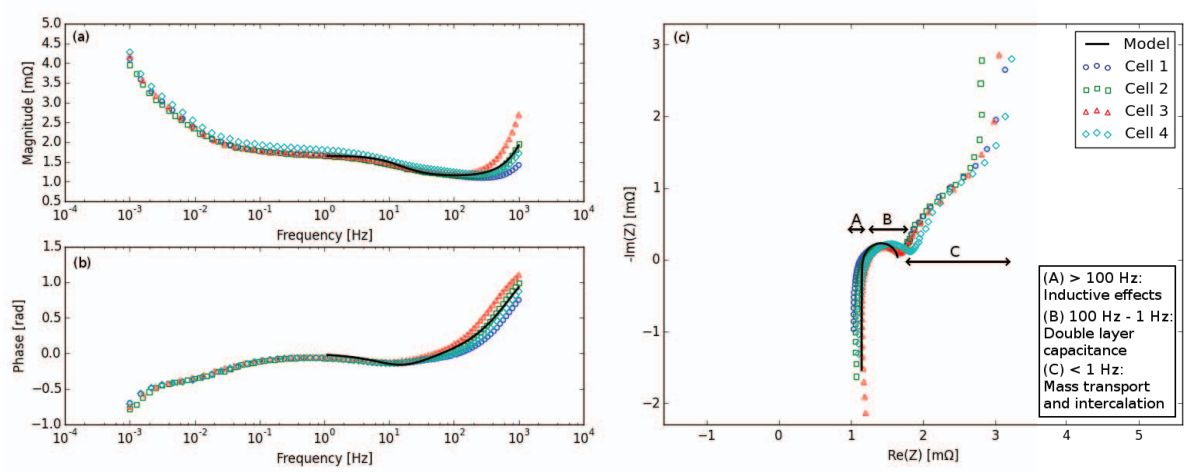

Figure 7: Experimental impedance data from four fresh li-ion cells, with the modelled impedance superimposed.

At present, focus is put on the high frequency behavior, so the high frequency impedance data (equal to or exceeding 1 Hz) is fitted to the equivalent circuit in Figure 8, expressed by equation 3, in a least-squares sense using the scipy.optimize Python module. The resulting fit is also shown in Figure 7. The

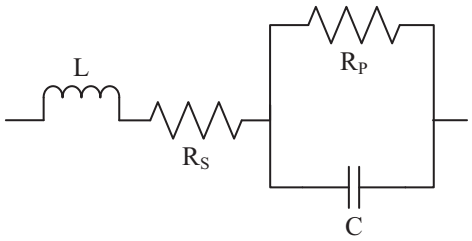

Figure 8: Equivalent circuit model.

impedance of this Z can be expressed as

$$Z = j\omega L + R_S + \frac{1}{j\omega C + \frac{1}{R_P}}. \tag{3}$$

The impedances of four fresh cells were averaged and used to determine the values of the parameters R_S, R_P, C, and L. The equivalent series resistance, parallel resistance, capacitance, and inductance of the fresh cells are reported in Table III.

Table III: Impedance of fresh li-ion cells

Cell	Series resistance ($m\Omega$)	Parallel resistance ($m\Omega$)	Capacitance (F)	Inductance (η H)
1	1.10	0.51	20.54	147
2	1.12	0.49	22.80	253
3	1.18	0.44	28.11	379
4	1.19	0.55	20.20	201
Average	1.15	0.50	22.92	254

4 Conclusions and Future Work

An experimental setup for investigating current ripple effects in li-ion battery cells is under construction in a joint project of KTH and Scania. To successfully accomplish the experimental setup requirements, a DCG was selected and adapted, a CRG was designed, and a methodology to ensure appropriate filter superposition was proposed. Numerical validations implemented in Matlab and PLECS of all the mentioned aspects were also accomplished. Additionally, aiming the experimental setup requirements, measurement procedures were proposed together with suited instrumentation.
In future work, the results of the current ripple effects in li-ion battery cells will then be compared with the fresh cell results above presented. The the experimental setup performance and its data quality will be analysed. After that, considerations and implications of such data will be explored.

References

[1] J. Du, M. Ouyang, and H. Wang, "Battery electric vehicle parameters design targeting to cost-benefit objective," in *2012 IEEE Vehicle Power and Propulsion Conference (VPPC)*, Oct. 2012, pp. 1160–1164.

[2] V.-S. Nguyen, V.-L. Tran, W. Choi, and D.-W. Kim, "Analysis of the output ripple of the DC-DC boost charger for Li-ion batteries," *Journal of Power Electronics*, vol. 14, no. 1, pp. 135–142, 2014.

[3] M. Liserre, F. Blaabjerg, and S. Hansen, "Design and control of an LCL-filter-based three-phase active rectifier," *IEEE Transactions on Industry Applications*, vol. 41, no. 5, pp. 1281–1291, Sep. 2005.

[4] S. De Breucker, K. Engelen, R. D'hulst, and J. Driesen, "Impact of Current Ripple on Li-Ion Battery Ageing," in *EVS27*, Barcelona, Spain, Nov. 2013.

[5] L.-R. Chen, S.-L. Wu, D.-T. Shieh, and T.-R. Chen, "Sinusoidal-ripple-current charging strategy and optimal charging frequency study for li-ion batteries," *IEEE Transactions on Industrial Electronics*, vol. 60, no. 1, pp. 88–97, Jan. 2013.

[6] Y.-D. Lee and S.-Y. Park, "Electrochemical state-based sinusoidal ripple current charging control," *IEEE Transactions on Power Electronics*, vol. 30, no. 8, pp. 4232–4243, Aug. 2015.

[7] N. Kularatna, "Dynamics and modeling of rechargeable batteries: what electrochemists? work tells the electronic engineers," *IEEE Power Electronics Magazine*, vol. 1, no. 4, pp. 23–33, Dec. 2014.

[8] T. Baumhöfer, M. Brühl, S. Rothgang, and D. U. Sauer, "Production caused variation in capacity aging trend and correlation toinitial cell performance," *Journal of Power Sources*, vol. 247, pp. 332–338, Feb. 2014.

[9] S. Bhide and Taehyun Shim, "Development of improved Li-ion battery model incorporating thermal and rate factor effects," in *2009 IEEE Vehicle Power and Propulsion Conference (VPPC), 7-10 Sept. 2009*, ser. 2009 IEEE Vehicle Power and Propulsion Conference (VPPC). IEEE, 2009, pp. 544–50.

[10] T. G. Zavalis, M. Klett, M. H. Kjell, M. Behm, R. W. Lindström, and G. Lindbergh, "Aging in lithium-ion batteries: Model and experimental investigation of harvested LiFePO4 and mesocarbon microbead graphite electrodes," *Electrochimica Acta*, vol. 110, pp. 335–348, Nov. 2013.

[11] P. Svens, J. Lindstrom, O. Gelin, M. Behm, and G. Lindbergh, "Novel field test equipment for lithium-ion batteries in hybrid electrical vehicle applications," *Energies*, vol. 4, no. 5, pp. 741–757, Apr. 2011.